Effect of proton energy on damage generation in irradiated silicon

S. Väyrynen[a] and J. Räisänen
Department of Physics, University of Helsinki, P.O. Box 64, FI-00014, Finland

(Received 24 November 2009; accepted 24 February 2010; published online 27 April 2010)

Czochralski- and float-zone- grown silicon detectors were irradiated with 2 to 5 MeV protons. Capacitance-voltage (*CV*) measurements served to deduce the effective doping profiles and current-voltage (*IV*) measurements served to obtaining information on irradiation-induced deep levels. The *CV* measurements show that the proton-induced net space charge is positive or negative depending on the energy of the bombarding ion. The commonly employed nonionizing energy loss hypothesis was tested with the low energy proton regime and prominent previously unobserved deviations from predictions were noted. © *2010 American Institute of Physics*. [doi:10.1063/1.3371714]

I. INTRODUCTION

Various types of irradiations have been used over the years to study particle bombardment-induced effects on materials. Typically, the chosen irradiation energy has been sufficiently high to permit particles to pass through the detector, thus inducing nearly uniform defect distributions. In several of these irradiation experiments, which employ mega-electron-volt protons, researchers have observed a space charge sign inversion for initially n-type silicon.[1–3] However, in other studies,[4,5] the bombarding particles have stopped in the silicon material and high concentrations of positive space charge have been observed in the end-of-range region.

Many irradiation-induced defects are electrically active and fabricating a diodelike structure (pn-junction) of the material to be studied makes defect-related studies of silicon feasible with, for example, deep-level transient spectroscopy as well as capacitance-voltage (*CV*) and current-voltage (*IV*) techniques. The *IV* method is sensitive only to defects with levels close to the mid-band gap. In the present study, *CV* measurements are feasible upto a bias of 600 V. This enables the full depletion of a reverse-biased diode structure processed from commonly available silicon wafers (thickness ~ 300 μm, resistivity > 1 kΩ), which thereby allows irradiations with higher-energy protons penetrating deeper into the detector. The depth-sensitive *CV* method is combined with *IV* data to enable the determination of heterogeneous current-related damage distributions.

Current-related damage induced by particle bombardment is usually scaled to other irradiation environments by using the nonionizing energy loss (NIEL) hypothesis.[6] We aimed to determine the sign of the net space charge of the induced major defects and to test the applicability of the NIEL hypothesis at relatively low energies by irradiating detectors made from Czochralski (Cz)- and float-zone (Fz)-grown silicon with 2 to 5 MeV protons.

II. MATERIALS AND EXPERIMENTS

To study irradiation-induced defects in silicon with the capacitance-voltage and current-voltage methods, detectors with diode structure ($p^+/n^-/n^+$) were fabricated from n-type, 300-μm thick, Cz-grown (Cz-Si, resistivity ~ 1 kΩ cm) and Fz-grown (Fz-Si, resistivity ~ 10 kΩ cm) materials supplied by Okmetic Ltd and Topsil, respectively. The detectors were processed at the Microelectronics Center of the Helsinki University of Technology. The thickness of the boron-implanted p^+ layer was about 3.5 μm and that of the phosphorus-implanted n^+ layer was about 7 μm. The front electrode was aluminum-sintered to a thickness of 0.5 μm. The detector active area was 5×5 mm^2 which was surrounded by 16 floating guard rings. A more detailed description of the detector structure is provided in Ref. 7. The current-voltage characteristics were determined with a Keithley 2410 SourceMeter Unit. The leakage current level at full depletion for all nonirradiated detectors was 30 to 100 nA. The capacitance-voltage characteristics were determined with a capacitance meter (frequency 18 kHz, maximum bias voltage 600 V) constructed especially for the measurement of diodes with a high leakage current. With the *CV* technique, a bulk donor concentration (N_D) of 5.3×10^{12} cm^{-3} was noted for the non-irradiated Cz detectors. For the Fz detectors, the corresponding value was $N_D = 5.1 \times 10^{11}$ cm^{-3}.

The Cz detectors, two pieces per selected energy, were irradiated from p^+-side with 2, 2.5, 3, 4, or 5 MeV protons and the Fz detectors with 2 or 2.5 MeV protons, respectively. The irradiations were performed using the 5 MV tandem accelerator of the Department of Physics, University of Helsinki. A detailed description of the irradiation facility used is provided in Refs. 8 and 9. Each detector was irradiated to the fluence of $(5.0 \pm 0.5) \times 10^{11}$ p/cm^2. All irradiations and measurements were performed at room temperature (21.5 ± 0.5 °C).

After irradiation, all detectors were annealed at room temperature for five days before making the *CV* and *IV* measurements. The *CV* curves measured for the irradiated Fz and Cz detectors are shown in Fig. 1(a), and typical *IV* curves in Fig. 1(b). The particles that stop in the detectors cause the levels noted in the *CV* curves, and the height of the level depends on the energy of the bombarding proton. In addition, as may be noted from Fig. 2, the width of the plateau depends on the irradiation fluence. Furthermore, clear changes

[a]Author to whom correspondence should be addressed. Electronic mail: samuli.vayrynen@helsinki.fi.

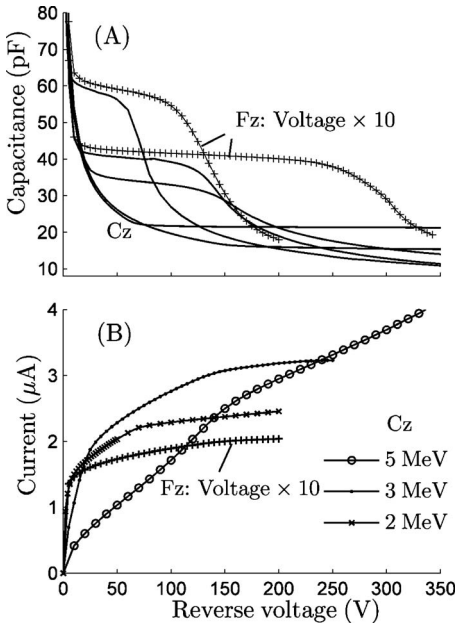

FIG. 1. (a) *CV* curves measured for Cz (solid lines) and Fz (lines with symbols) detectors after proton irradiation at various energies. The curves with the plateau at the highest capacitance value (~60 pF) refer to 2 MeV irradiations and those having the plateau at the lowest value (~16 pF) to 5 MeV irradiations. The curves in between correspond to 2.5, 3, and 4 MeV irradiations. For the sake of clarity, the voltage values of the Fz detectors (2 and 2.5 MeV irradiations) have been multiplied by a factor of 10. (b). Typical *IV* curves obtained after irradiation at selected energies. The curve for the Fz detector refers to a 2 MeV irradiation.

in the slopes of the *IV* curves perfectly match the plateau turning points in the corresponding *CV* curves.

III. THEORETICAL CONSIDERATIONS

From the *CV* characteristics measured, one can determine the effective doping concentration (N_{eff}) as a function of depth at the low-doped side of the pn junction.[10] At the edge of the depletion region in the reverse-biased p^+n junction, the effective doping concentration can be calculated from

$$N_{\text{eff}}(x) = \frac{2}{e\varepsilon_r\varepsilon_0}\left(\frac{dC_j^{-2}}{dV}\right)^{-1}, \tag{1}$$

where e is the elementary charge, ε_r is the relative permittivity of silicon (the value adopted in this study was 11.7), ε_0 is the permittivity of a vacuum, C_j is the junction capacitance

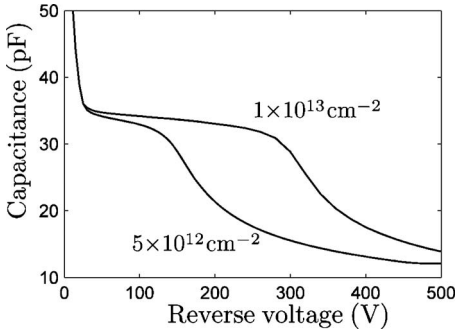

FIG. 2. The effect of irradiation fluence on *CV* curve plateau width. The material is Cz-grown silicon and the bombarding proton energy is 3 MeV.

per unit area, and V is the applied bias. The depletion layer width (x) is obtained simply from Eq. (2)

$$C_j(V) = \frac{\varepsilon_r\varepsilon_0}{x(V)}. \tag{2}$$

The reverse current density J_R of an irradiated pn junction is the sum of four components, the diffusion current J_{diff}, the current generated at the surface J_{sg}, the current J_g generated in the depleted layer, and the secondary ionization current J_{ii} at high reverse voltages. The diffusion current and the current generated at the surface can be eliminated by subtracting the *IV* curve measured prior to irradiation from the curve obtained after irradiation. The current must be subtracted relative to depth, thus correspondence between voltage and depth is required. This is obtained from the *CV* data by using Eq. (2). The component J_{ii} cannot be eliminated easily but fortunately it dominates only near the breakdown voltages.

The generation current strongly depends on the concentration of defects with deep energy levels (i.e., levels close to the mid-band gap). The defect concentration depends on the irradiation fluence and experimental results indicate that the following linear relationship between the generation current and fluence holds:[6]

$$\frac{\Delta I}{V} = \alpha\Phi_{neq}, \tag{3}$$

where ΔI is the current change in volume V, α is the current-related damage rate, and Φ_{neq} is the 1 MeV neutron equivalent irradiation fluence. Proton fluencies Φ_p are scaled to a 1 MeV neutron equivalent fluence using hardness factor κ (i.e., $\Phi_{neq}=\kappa\Phi_p$, NIEL scaling hypothesis[6]). Typically, Eq. (3) is used in situations where the bombarding energy of the incident particles is sufficient to enable penetration through the detector, thus resulting in nearly uniform defect distributions. There[6] are essentially no constraints on the proton energy in Eq. (3).

Using the depth information obtained from the *CV* data, the *IV* data enable us the opportunity to calculate the current density dJ_g generated in a layer dx at the edge of the depletion area. Equation (3) may be expressed as

$$\left.\frac{dJ_g}{dx}\right|_x = \alpha(x)\kappa(x)\Phi_p. \tag{4}$$

Because the stopping power of silicon for protons is well established,[11] depth dependency may be converted to energy dependency.

On the other hand, the generation current density J_g in the depletion region of the p^+n junction can be expressed as[12]

$$J_g = e\int_0^W G\,dx \cong \frac{en_iW}{\tau_g}, \tag{5}$$

where G is the rate of electron-hole pair generation, n_i is the intrinsic carrier concentration, and τ_g is the generation lifetime. For a thin layer dx, Eq. (5) yields

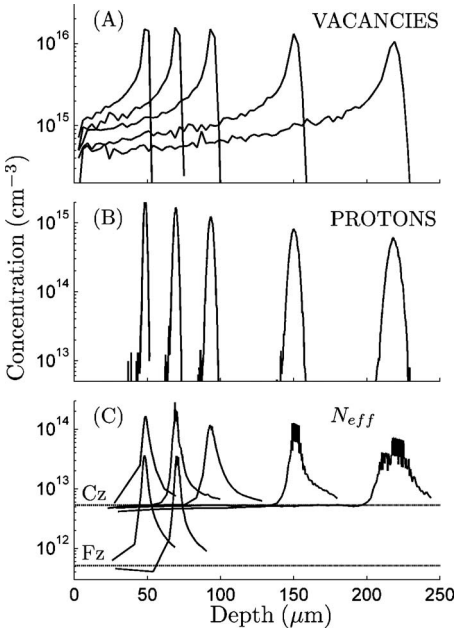

FIG. 3. Comparison of the calculated vacancy (a) and proton (b) depth profiles with the effective doping profiles (c) obtained from the *CV* data. The profiles refer to irradiation energies of 2, 2.5, 3, 4, and 5 MeV (from left to right). For each irradiation and calculation, the fluence has been 5×10^{11} p/cm^{-2}. The horizontal dashed lines in the lowest graph indicate the doping levels (5.3×10^{12} cm^{-3} and 5.1×10^{11} cm^{-3}) prior to irradiation. Note that, for the Cz detectors, the N_{eff} curves below the initial donor concentration level do not overlap and the lowest N_{eff} value refers to the highest bombarding energy.

$$\left.\frac{dJ_g}{dx}\right|_x = \frac{en_i}{\tau_g(x)}. \tag{6}$$

The depth variable can be converted to energy E, as in the case of Eq. (4).

IV. RESULTS AND DISCUSSION

Applying Eqs. (1) and (2) to the measured *CV* data the depth profiles of N_{eff} were extracted. The deduced profiles are shown in Fig. 3 and are compared in relation to the implanted proton and vacancy distributions obtained by the srim (Ref. 11) calculations. The inactive layer (~4 μm Si equivalent) in front of the depleted layer has been taken into account in defining the positions of the measured profiles.

According to Fig. 3, the effective doping profiles show no diminishing concentration tail when shifting from the profile peak toward the surface. Even if the N_{eff} profiles are approximately twice as wide as the corresponding proton distributions, their shapes in general more closely match the vacancy profiles. It should be noted that the N_{eff} profiles measured also feature deep-end tails extending beyond the end-of-range region, possibly due to the diffusion of defects resulting from the large concentration gradient at the deep-end side of the peak[13] or to bombarding proton channelling in silicon.

An important finding is that the concentrations of N_{eff} close to the surface are lower than the donor concentration of the nonirradiated material. But deeper, near the end-of-range region, they are higher. For the Cz detectors the depth in silicon where the net space charge changes from negative to positive, is about 40 μm for 2.5 MeV, ~60 μm for 3 MeV, ~110 μm for 4 MeV, and ~170 μm for 5 MeV irradiated detector. These values refer to a distance of 27 to 47 μm from the end-of-range region toward the detector surface.

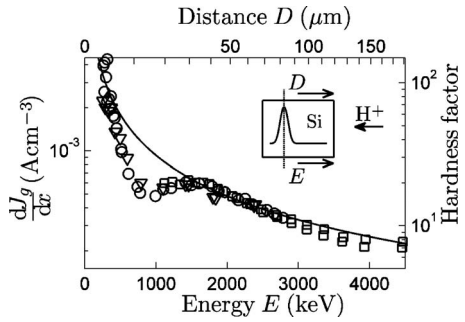

FIG. 4. Change in current density as a function of proton energy compared to relative damage concentration estimated by the NIEL scaling hypothesis (solid line, right axis). The results obtained from the data on the 5 MeV irradiations are shown by the squares, data on the 4 MeV irradiations as circles, and data on the 3 MeV irradiations as triangles. The distance D from the projected range value to the detector surface, as calculated by the SRIM code, is provided on the top axis and is explained in the inset.

Some researchers have proposed that the change of the net space charge is caused mainly by the differing defect levels created in the end-of-range region and in the region closer to the detector surface. This assumption is in agreement with the findings of reference,[14] where the mega-electron-volt proton-induced defects have been grouped into two categories, those created in the near surface region and those created near the end-of-range region.

The current density derivative dJ_g/dx is proportional to $\alpha(E)\kappa(E)$ and inversely proportional to the generation lifetime τ_g [Eqs. (4) and (6)]. The dJ_g/dx values measured as a function of proton energy are illustrated in Fig. 4 for the Cz material. For comparison, the NIEL scaling hypothesis (hardness factor κ) and the vacancy production curve provided by the SRIM calculations are also shown. For Fz material, the depletion depth corresponding to the projected range is achieved by a bias voltage as low as 1 V [Fig. 1(a)], consequently, the dJ_g/dx values are not presented.

As Fig. 4 shows, the NIEL scaling hypothesis and SRIM damage calculations agree well with the present experimental data for energies above 1700 keV but a clear discrepancy may be noted at lower energies. For energies above 1700 keV the value for the α parameter is about 6×10^{-18} A cm^{-1} assuming that the NIEL hypothesis is valid [Eq. (4)]. The current density derivative seems to saturate at energies between 1700 and 700 keV. The latter value corresponds to the end-of-range region of the bombarding protons. The transition point (1700 keV) is located at an approximate distance of 37 μm from the projected range, which is in close agreement with the value noted for the position, in which the net space charge type changes. The saturation of the defect concentration noted[15] at the end-of-range region, could also take place in a region closer to the detector surface. Moreover, we propose that the interaction of more complex defects and the recombination of electron-hole pairs decrease the generated bulk current, which may lead to the noted observation. In composing Fig. 4, a con-

stant fluence $[(5.0\pm0.5)\times10^{11}\ \mathrm{p/cm^2}]$ has been assumed at all depths. This assumption is not valid in regions less than 10 μm from the projected range R_p, where a significant proportion of the protons have stopped (end-of-range region). Thus, the $\mathrm{d}J_g/\mathrm{d}x$ is underestimated in the end-of-range region.

In this context, we have knowingly avoided the separation of the $\alpha(E)\kappa(E)$ factor. As noted, for energies above 1700 keV, the NIEL scaling agrees with the measurements leading to the assumption that α is the sole variable in Eq. (4). However, studies cited in Ref. 16 indicate that factor κ deviates from the NIEL predictions at higher proton energies (7–10 MeV), and others in Ref. 17 have noted deviations at lower energies also (100 keV$<E<$6 MeV). The generation lifetime measurements[18] carried out using the Zerbst technique (which is based on capacitance measurements) for 4 MeV proton-irradiated silicon have shown that the τ_g behavior agrees with the SRIM defect calculations near the end-of-range region as well, which contradicts the present results shown in Fig. 4. In general, the main problem in studying the hardness factor is the varying array of methods used.[19]

V. CONCLUDING REMARKS

This paper reports our findings on the damage profiles in silicon caused by MeV proton bombardment. The effective doping concentration profiles have been measured with the *CV* method and the current-related damage was studied with the *IV* technique. The resulting defects can be categorized into two main groups, defects with net negative space charge induced by protons with energies above 1700 keV and defects with positive net space charge induced by lower-energy protons. In addition, the (hydrogen-related) end-of-range defects could be distinguished from the defects with positive charge. In the p-type region the creation of current-related damage follows well the predictions of the empirical model [Eq. (3)]. However, in the n-type region, the production of damage seems to saturate with a high concentration of current-related damage created prior to the end-of-range region. The probable main causes of the noted phenomena are the energy dependency of the type of the net space charge generated and the interactions of the defects.

ACKNOWLEDGMENTS

The authors would like to thank Dr Esa Tuovinen for processing the detectors and the Helsinki Institute of Physics for providing the *CV* and *IV* measurement units. The financial support of the Finnish Society of Science and Letters, the Magnus Ehrnrooth Foundation and the Academy of Finland (Project No. 132128) is gratefully acknowledged.

[1] K. Leinonen, T. Palviainen, T. Tuuva, E. Tuovinen, J. Härkönen, and P. Luukka, Nucl. Instrum. Methods Phys. Res. A **552**, 357 (2005).
[2] N. Manna, D. Bassignana, M. Boscardin, L. Borrello, M. Bruzzi, D. Creanza, M. de Palma, V. Eremin, A. Macchiolo, D. Menichelli, A. Messineo, V. Radicci, M. Scaringella, and E. Verbiskaya, Nucl. Instrum. Methods Phys. Res. A **583**, 87 (2007).
[3] J. Härkönen, E. Tuovinen, P. Luukka, E. Tuominen, K. Lassila-Perini, P. Mehtälä, S. Nummela, J. Nysten, A. Zibellini, Z. Li, E. Fretwurst, G. Lindstroem, J. Stahl, F. Hönniger, V. Eremin, A. Ivanov, E. Verbitskaya, P. Heikkilä, V. Ovchinnikov, M. Yli-Koski, P. Laitinen, A. Pirojenko, I. Riihimäki, and A. Virtanen, Nucl. Instrum. Methods Phys. Res. A **518**, 346 (2004).
[4] P. Desgardin, L. Henry, E. Ntsoenzok, G. Blondiaux, J. F. Barbot, and C. Blanchard, Nucl. Instrum. Methods Phys. Res. B **127–128**, 59 (1997).
[5] P. Hazdra and V. Komarnitskyy, IET Circuits Devices Syst. **1**, 321 (2007).
[6] G. Lindström, Nucl. Instrum. Methods Phys. Res. A **512**, 30 (2003).
[7] S. Väyrynen, J. Räisänen, I. Kassamakov, and E. Tuominen, J. Appl. Phys. **106**, 104914 (2009).
[8] S. Väyrynen, P. Pusa, P. Sane, P. Tikkanen, J. Räisänen, K. Kuitunen, F. Tuomisto, J. Härkönen, I. Kassamakov, E. Tuominen, and E. Tuovinen, Nucl. Instrum. Methods Phys. Res. A **572**, 978 (2007).
[9] S. Väyrynen, J. Räisänen, P. Tikkanen, I. Kassamakov, and E. Tuominen, J. Appl. Phys. **106**, 024908 (2009).
[10] G. Lutz, *Semiconductor Particle Detectors* (Springer-Verlag, Berlin, 1999).
[11] J. F. Ziegler, SRIM software package http://www.srim.org/.
[12] S. M. Sze, *Semiconductor devices, Physics and Technology* (Wiley, New York, 1985).
[13] N. Keskitalo and A. Hallén, Solid-State Electron. **37**, 55 (1994).
[14] W. Wondrak, K. Bethge, and D. Silber, J. Appl. Phys. **62**, 3464 (1987).
[15] J. F. Barbot, E. Ntsoenzok, C. Blanchard, J. Vernois, and D. B. Isabelle, Nucl. Instrum. Methods Phys. Res. B **95**, 213 (1995).
[16] D. Bechevet, M. Glaser, A. Houdayer, C. Lebel, C. Leroy, M. Moll, and P. Roy, Nucl. Instrum. Methods Phys. Res. A **479**, 487 (2002).
[17] S. R. Messenger, E. A. Burke, G. P. Summers, and R. J. Walters, IEEE Trans. Nucl. Sci. **49**, 2690 (2002).
[18] N. Q. Khánh, C. Kovácsics, T. Mohácsy, M. Ádám, and J. Gyulai, Nucl. Instrum. Methods Phys. Res. B **147**, 111 (1999).
[19] A. Vasilescu and G. Lindström, *Notes on the fluence normalisation based on the NIEL scaling hypothesis* (ROSE/TN/2000–02, 2000).